

# Laser cooling and trapping of potassium at magic wavelengths

M. S. Safronova<sup>1,2</sup>, U. I. Safronova<sup>3,4</sup>, and Charles W. Clark<sup>2</sup>

<sup>1</sup>*Department of Physics and Astronomy, 217 Sharp Lab,  
University of Delaware, Newark, Delaware 19716*

<sup>2</sup>*Joint Quantum Institute, National Institute of Standards and Technology  
and the University of Maryland, Gaithersburg, Maryland 20899-8410, USA*

<sup>3</sup>*Physics Department, University of Nevada, Reno, Nevada 89557*

<sup>4</sup>*Department of Physics, University of Notre Dame, Notre Dame, Indiana 46556*

We carry out a systematic study of the static and dynamic polarizabilities of the potassium atom using a first-principles high-precision relativistic all-order method in which all single, double, and partial triple excitations of the Dirac-Fock wave functions are included to all orders of perturbation theory. Recommended values are provided for a large number of electric-dipole matrix elements. Static polarizabilities of the  $4s$ ,  $4p_j$ ,  $5s$ ,  $5p_j$ , and  $3d_j$  states are compared with other theory and experiment where available. We use the results of the polarizability calculations to identify magic wavelengths for the  $4s - np$  transitions for  $n = 4, 5$ , *i.e.* those wavelengths for which the two levels have the same ac Stark shifts. These facilitate state-insensitive optical cooling and trapping. The magic wavelengths for the  $4s - 5p$  transitions are of particular interest for attaining a quantum gas of potassium at high phase-space density. We find 20 such wavelengths in the technically interest region of 1050 – 1130 nm. Uncertainties of all recommended values are estimated.

PACS numbers: 31.15.ac, 37.10.De, 31.15.ap, 31.15.bw

## I. INTRODUCTION

Due to their applications in ultra-precise atomic clocks, degenerate quantum gases and quantum information, the magic wavelengths of atoms have become a subject of great interest in both experiments [1–4] and theory [5–15]. The energy levels of atoms trapped in a light field are shifted by an amount that is proportional to their frequency-dependent polarizability, so the difference in the energies of any two levels depends upon the trapping field. This difference is often called the “ac Stark shift”.

The idea of a “magic” wavelength,  $\lambda_{\text{magic}}$ , at which there is no relative shift of a given pair of energy levels, was first proposed in Refs. [16, 17] in the context of optical atomic clocks. An atom confined in a trap constructed of light with a magic wavelength for the clock transition will, to lowest order, have the same transition energy as it does in free space.

This simple idea has a number of other applications. A problem arises in cooling and trapping schemes, where the ac Stark shift of the cooling or trapping transition may lead to heating. Recent experiments in  $^6\text{Li}$  [18] and  $^{40}\text{K}$  [2] degenerate quantum gases in optical traps demonstrated temperature reductions by a factor of about five and phase-space density increases by at least a factor of ten by laser cooling using ultraviolet (UV) transitions ( $2s - 3p$  and  $4s - 5p$ , respectively) compared to conventional cooling with the visible or infrared  $D_1$  and  $D_2$  transitions. However, the ac Stark shifts due to trap light must be nearly the same for both levels in the transition to allow for efficient and uniform cooling [18]. This is accomplished by building the optical trap using light with the magic wavelength for the corresponding UV transitions. The use of the magic wavelengths is also advanta-

geous for trapping and controlling atoms in high-Q cavities in the strong coupling regime, so as to minimize decoherence in quantum computation and communication protocols [19], and in the implementation of the Rydberg gate for quantum computing with neutral atoms [20, 21].

Variations on the magic wavelength idea include the use of multiple light fields to attain ac Stark shift targets [22] or to maximize differential response between different atomic species – for example, the “tune-out” wavelengths that trap one species but not another [23, 24]. Design and evaluation of all these applications requires accurate data on atomic frequency-dependent polarizabilities. One goal of our present work is to provide a list of all magic wavelengths for potassium UV  $4s - 5p_j$  transitions in regions that are convenient for laser cooling of ultracold gases to high phase-space densities. For example, in 2011, low-temperature high-density magneto-optical trapping of potassium using the open  $4s_{1/2} \rightarrow 5p_{3/2}$  transition at 405 nm was performed by McKay *et al.* [2]. Fermionic  $^{40}\text{K}$  was captured using a magneto-optical trap (MOT) on the closed  $4s \rightarrow 4p_{3/2}$  transition at 767 nm and then transferred, with high efficiency, to a MOT on the open  $4s \rightarrow 5p_{3/2}$  transition at 405 nm. Because the  $5p_{3/2}$  state has a smaller linewidth than the  $4p_{3/2}$  state, the Doppler limit is reduced from  $145\mu\text{K}$  to  $24\mu\text{K}$ , and temperatures as low as  $63(6)\mu\text{K}$  were observed.

In this paper we provide a list of magic wavelengths for the  $4s - 4p$  and  $4s - 5p$  transitions, calculate dc and ac polarizabilities for several low-lying states, and provide recommended values for a number of relevant electric-dipole transitions which are of interest to applications such as those described above. Where possible, we compare our results with available experimental [25] and high-precision theoretical values [26].

Some of the calculations reported here required evaluation of the electric-dipole matrix elements for very highly excited states, such as  $14s$ . These states are needed since the ac polarizabilities for the magic wavelengths of particular experimental interest (around 1050 nm) are dominated by the  $5p - nl$  transitions with  $n = 12 - 14$ . Such states were previously beyond the capabilities of the all-order method used here due to the large spatial extent of the orbitals. In this work, we resolved the numerical problems associated with such calculations and successfully demonstrated the stability of our new approach.

We begin with a brief review of recent research on the applications of magic wavelength concepts in Section II. The calculation of electric-dipole matrix elements, static and dynamic polarizabilities as well as their uncertainties is discussed in Section III. The magic wavelengths are discussed in Section IV.

## II. REVIEW OF MAGIC WAVELENGTH STUDIES

Up to the present, most work on magic wavelengths has been done on group I and group II atoms, which are the species most easily cooled and trapped by optical methods. We summarize these in turn. The following examples are representative of significant applications of the magic wavelength concept, however, these examples are not intended to constitute an exhaustive review.

### A. Group I

The cancellation of the differential ac Stark shift of the microwave hyperfine clock transition in trapped  $^{87}\text{Rb}$  atoms was demonstrated in [3]. The technique had implications for experiments involving the precise control of optically trapped neutral atoms, but the cancellation comes at the expense of a small magnetic-field sensitivity. ‘‘Doubly magic’’ conditions in magic-wavelength trapping of ultracold alkali-metal atoms were investigated by Derevianko [5]. This work demonstrated that the microwave transitions in alkali-metal atoms may be indeed made impervious to both trapping laser intensity and fluctuations of magnetic fields.

The issue of the mismatch of the polarizabilities of the ground and excited states has also arisen in the Rydberg gate approach to quantum information processing [27, 28], in which the qubit is based on two ground hyperfine states of neutral atoms confined in an optical lattice. An atom in a Rydberg state will, in general, move in a different optical lattice potential than that experienced by the ground state. Therefore, the vibrational state of the atom in the lattice may change after the gate operation is completed, leading to decoherence due to motional heating. This problem may be resolved by the use of magic wavelengths [20, 21]. Use of magic wavelengths in optical traps for Rydberg atoms was also discussed in [8],

where three designs for blue-detuned dipole traps were presented.

Magic wavelengths for the alkali-metal atoms from Na to Cs, for which the  $ns$  and  $np_{1/2}$  or  $np_{3/2}$  atomic levels have the same ac Stark shifts, were evaluated by Arora *et al.* [14]. The case of circular polarization was considered in [30, 31]. McKeever *et al.* [19] demonstrated state-insensitive trapping of Cs atoms at 935 nm while maintaining a strong coupling for the  $6s_{1/2} - 6p_{3/2}$  transition. A bichromatic scheme for state-insensitive optical trapping of Rb atom was explored in Ref. [22]. In the case of Rb, the magic wavelengths associated with monochromatic trapping were sparse and relatively inconvenient. The bichromatic approach yielded a number of promising magic wavelength pairs. The precise magic wavelengths for Li  $2s - 2p_j$  and  $2s - 3p_j$  transitions in convenient wavelength regions were recently calculated in [32]. The results were presented for both  $^6\text{Li}$  and  $^7\text{Li}$  to illustrate the possibilities for differential light shifts between the two isotopes.

### B. Group II

The magic wavelengths for the Sr  $5s^2\ ^1S_0 - 5s5p\ ^3P_0^\circ$  and  $5s^2\ ^1S_0 - 5s5p\ ^3P_1^\circ$  transitions have been measured in [33, 34]. The Yb clock  $6s^2\ ^1S_0 - 6s6p\ ^3P_0^\circ$  magic wavelength was predicted to be 752 nm in [35] and measured to be 759.355 nm in Ref. [36]. The magic wavelength for the ultraviolet  $6s^2\ ^1S_0 \leftrightarrow 6s6p\ ^3P_0^\circ$  clock transition in Hg was recently reported by Yi *et al.* [1]. The Stark-free (magic) wavelength was found to be 362.53(0.21) nm, in excellent agreement with the theoretical prediction 360 nm from [37], calculated using a method that combines configuration interaction and many-body perturbation theory. The magic wavelengths of other group II and group IIb atoms have been predicted in [38]. The magic wavelengths are very sensitive to the values of the ac polarizabilities and allow for precise tests of the theory [39, 40]. Moreover, the magic wavelengths can be used to determine the values of important electric-dipole matrix elements which are difficult to obtain by direct experimental techniques. For example, the  $5s5p\ ^3P_0^\circ - 5s6s\ ^3S_1$  matrix element in Sr was recently determined using the experimental value of the Sr  $5s^2\ ^1S_0 - 5s5p\ ^3P_0^\circ$  magic wavelength with 0.5% precision [40]. Dammalapati *et al.* [9] investigated light shifts of heavy alkaline earth elements barium (Ba) and radium (Ra), which are of interest for development of optical lattice clocks and for permanent electric dipole moment searches. The wavelength dependence of light shifts of the  $ns^2\ ^1S_0$  ground state, the  $nsnp\ ^3P_1^\circ$  and  $ns(n-1)d\ ^1D_2$  excited states in Ba ( $n = 6$ ) and the  $ns^2\ ^1S_0$  ground state, the  $nsnp\ ^3P_1^\circ$  and  $ns(n-1)d\ ^3D_2$  excited states in Ra ( $n = 7$ ) were calculated. Several magic wavelengths in the visible and infrared regions accessible with commercial lasers for optical dipole trapping of Ba and Ra were identified [9]. Magic wavelengths of an optical clock transition of bar-

TABLE I: Absolute values of the reduced electric-dipole matrix elements in K and their uncertainties in a.u.. The present all-order values are given unless noted otherwise. <sup>(a)</sup>Expt. [29], <sup>(b)</sup>determined from Stark shift data in [14]. The uncertainties are estimated where possible (see text).

Transition	Value	Transition	Value	Transition	Value	Transition	Value
$4s - 4p_{1/2}$	4.106(4) <sup>(a)</sup>	$5s - 4p_{1/2}$	3.885(8)	$4s - 4p_{3/2}$	5.807(7) <sup>(a)</sup>	$5s - 4p_{3/2}$	5.54(1)
$4s - 5p_{1/2}$	0.2755	$5s - 5p_{1/2}$	9.49(3)	$4s - 5p_{3/2}$	0.4060	$5s - 5p_{3/2}$	13.40(4)
$4s - 6p_{1/2}$	0.0855	$5s - 6p_{1/2}$	0.90(1)	$4s - 6p_{3/2}$	0.1302	$5s - 6p_{3/2}$	1.30(2)
$4s - 7p_{1/2}$	0.0390	$5s - 7p_{1/2}$	0.3347	$4s - 7p_{3/2}$	0.0614	$5s - 7p_{3/2}$	0.4907
$4s - 8p_{1/2}$	0.0225	$5s - 8p_{1/2}$	0.183(3)	$4s - 8p_{3/2}$	0.0364	$5s - 8p_{3/2}$	0.271(4)
$4s - 9p_{1/2}$	0.0147	$5s - 9p_{1/2}$	0.120(2)	$4s - 9p_{3/2}$	0.0244	$5s - 9p_{3/2}$	0.178(3)
$4s - 10p_{1/2}$	0.0105	$5s - 10p_{1/2}$	0.087(1)	$4s - 10p_{3/2}$	0.0177	$5s - 10p_{3/2}$	0.129(2)
$4p_{1/2} - 6s$	0.903(4)	$5p_{1/2} - 6s$	8.79(2)	$4p_{3/2} - 6s$	1.279(5)	$5p_{3/2} - 6s$	12.50(2)
$4p_{1/2} - 7s$	0.476(2)	$5p_{1/2} - 7s$	1.801(8)	$4p_{3/2} - 7s$	0.673(3)	$5p_{3/2} - 7s$	2.54(1)
$4p_{1/2} - 8s$	0.314(2)	$5p_{1/2} - 8s$	0.912(5)	$4p_{3/2} - 8s$	0.444(2)	$5p_{3/2} - 8s$	1.287(7)
$4p_{1/2} - 9s$	0.230(1)	$5p_{1/2} - 9s$	0.592(3)	$4p_{3/2} - 9s$	0.325(2)	$5p_{3/2} - 9s$	0.834(4)
$4p_{1/2} - 10s$	0.1791(9)	$5p_{1/2} - 10s$	0.430(2)	$4p_{3/2} - 10s$	0.253(1)	$5p_{3/2} - 10s$	0.607(3)
$4p_{1/2} - 11s$	0.1452(8)	$5p_{1/2} - 11s$	0.334(2)	$4p_{3/2} - 11s$	0.205(1)	$5p_{3/2} - 11s$	0.471(3)
$4p_{1/2} - 3d_{3/2}$	7.979(35) <sup>(b)</sup>	$5p_{1/2} - 3d_{3/2}$	7.2(1)			$5p_{3/2} - 3d_{3/2}$	3.19(5)
$4p_{1/2} - 4d_{3/2}$	0.1121(8)	$5p_{1/2} - 4d_{3/2}$	17.04(6)	$4p_{3/2} - 4d_{3/2}$	0.0400(1)	$5p_{3/2} - 4d_{3/2}$	7.64(3)
$4p_{1/2} - 5d_{3/2}$	0.333(2)	$5p_{1/2} - 5d_{3/2}$	0.931(4)	$4p_{3/2} - 5d_{3/2}$	0.155(1)	$5p_{3/2} - 5d_{3/2}$	0.398(2)
$4p_{1/2} - 6d_{3/2}$	0.341(3)	$5p_{1/2} - 6d_{3/2}$	0.063(6)	$4p_{3/2} - 6d_{3/2}$	0.157(1)	$5p_{3/2} - 6d_{3/2}$	0.039(3)
$4p_{1/2} - 7d_{3/2}$	0.298(2)	$5p_{1/2} - 7d_{3/2}$	0.219(5)	$4p_{3/2} - 7d_{3/2}$	0.136(1)	$5p_{3/2} - 7d_{3/2}$	0.105(3)
$4p_{1/2} - 8d_{3/2}$	0.254(2)	$5p_{1/2} - 8d_{3/2}$	0.236(4)	$4p_{3/2} - 8d_{3/2}$	0.116(1)	$5p_{3/2} - 8d_{3/2}$	0.111(2)
$4p_{1/2} - 9d_{3/2}$	0.218(2)	$5p_{1/2} - 9d_{3/2}$	0.222(3)	$4p_{3/2} - 9d_{3/2}$	0.0995(8)	$5p_{3/2} - 9d_{3/2}$	0.103(2)
$4p_{3/2} - 3d_{5/2}$	10.734(47) <sup>(b)</sup>	$5p_{3/2} - 3d_{5/2}$	9.6(1)				
$4p_{3/2} - 4d_{5/2}$	0.1170(4)	$5p_{3/2} - 4d_{5/2}$	22.93(8)	$3d_{3/2} - 5p_{1/2}$	7.2(1)	$3d_{5/2} - 5p_{3/2}$	9.6(1)
$4p_{3/2} - 5d_{5/2}$	0.467(3)	$5p_{3/2} - 5d_{5/2}$	1.188(7)	$3d_{3/2} - 6p_{1/2}$	1.03(1)	$3d_{5/2} - 6p_{3/2}$	1.39(1)
$4p_{3/2} - 6d_{5/2}$	0.471(4)	$5p_{3/2} - 6d_{5/2}$	0.119(8)	$3d_{3/2} - 7p_{1/2}$	0.497(5)	$3d_{5/2} - 7p_{3/2}$	0.673(7)
$4p_{3/2} - 7d_{5/2}$	0.409(3)	$5p_{3/2} - 7d_{5/2}$	0.318(7)	$3d_{3/2} - 8p_{1/2}$	0.317(3)	$3d_{5/2} - 8p_{3/2}$	0.428(4)
$4p_{3/2} - 8d_{5/2}$	0.349(3)	$5p_{3/2} - 8d_{5/2}$	0.335(6)	$3d_{3/2} - 9p_{1/2}$	0.228(3)	$3d_{5/2} - 9p_{3/2}$	0.308(4)
$4p_{3/2} - 9d_{5/2}$	0.299(2)	$5p_{3/2} - 9d_{5/2}$	0.312(4)	$3d_{3/2} - 10p_{1/2}$	0.176(2)	$3d_{5/2} - 10p_{3/2}$	0.238(3)
$3d_{3/2} - 4p_{3/2}$	3.578(16) <sup>(b)</sup>	$3d_{3/2} - 4f_{5/2}$	12.3(2)	$3d_{5/2} - 4f_{7/2}$	14.6(2)	$3d_{5/2} - 4f_{5/2}$	3.27(4)
$3d_{3/2} - 5p_{3/2}$	3.19(5)	$3d_{3/2} - 5f_{5/2}$	4.92(2)	$3d_{5/2} - 5f_{7/2}$	5.88(3)	$3d_{5/2} - 5f_{5/2}$	1.315(6)
$3d_{3/2} - 6p_{3/2}$	0.464(5)	$3d_{3/2} - 6f_{5/2}$	2.899(8)	$3d_{5/2} - 6f_{7/2}$	3.465(0)	$3d_{5/2} - 6f_{5/2}$	0.775(2)
$3d_{3/2} - 7p_{3/2}$	0.224(2)	$3d_{3/2} - 7f_{5/2}$	2.001(5)	$3d_{5/2} - 7f_{7/2}$	2.392(6)	$3d_{5/2} - 7f_{5/2}$	0.535(1)
$3d_{3/2} - 8p_{3/2}$	0.143(1)						
$3d_{3/2} - 9p_{3/2}$	0.103(1)						
$3d_{3/2} - 10p_{3/2}$	0.079(1)						

ium were presented in [10]. Dipole polarizabilities of  $ns^2\ ^1S_0$  and  $nsnp\ ^3P_0^o$  states and relevant magic wavelengths of Sr, Yb, Zn, Cd, and Hg atoms were studied by a semiempirical approach in Refs. [12, 13].

The magic wavelength conditions that can make optical lattice clocks insensitive to atomic motion were presented by Katori *et al.* [6]. This work demonstrated that the spatial mismatch of the interactions in the clock transition can be treated as a spatially constant offset  $\delta\nu$  for specific lattice geometries. Numerical estimates were made for Sr [6].

Theoretical study of the dynamic scalar polarizabilities of the ground and selected long-lived excited states of dysprosium was recently carried out by Dzuba *et al.* [7]. A set of the magic wavelengths of the unpolarized lattice laser field for each pair of states, which includes the ground state and one of these excited states was given. The authors presented an analytical formula that allows

for the determination of approximate values of the magic wavelengths without calculating the dynamic polarizabilities of the excited states near resonances [7].

### III. MATRIX ELEMENTS AND POLARIZABILITIES

The magic wavelengths for a specific transition are located by calculating the frequency-dependent polarizabilities of the lower and upper states and finding their crossing points. The all-order approach to the calculation of atomic polarizabilities was discussed in Refs. [14, 24, 26, 32, 43, 44], and we provide only a brief summary of the methods here. Unless stated otherwise, all specific data refers to the K atom, and we use the conventional system of atomic units, a.u., in which  $e$ ,  $m_e$ ,  $4\pi\epsilon_0$  and the reduced Planck constant  $\hbar$  have the numer-

TABLE II: Values of scalar ( $\alpha_0$ ) and tensor ( $\alpha_2$ ) polarizabilities in K. The present results are compared with theoretical and experimental values. Ref. [26] did not include uncertainty estimates. All values are in atomic units.

	Present	Theory	Expt.
$\alpha_0(4s_{1/2})$	290.4(6)	290.2(8)[41]	290.8(1.4)[25]
$\alpha_0(5s_{1/2})$	4961(22)		
$\alpha_0(4p_{1/2})$	611(6)	604.1 [26]	587(87) [42]
$\alpha_0(4p_{3/2})$	620(5)	614.1[26]	613(103) [42]
$\alpha_0(5p_{1/2})$	7053(70)		
$\alpha_0(5p_{3/2})$	7230(61)		
$\alpha_0(3d_{3/2})$	1420(30)		
$\alpha_0(3d_{5/2})$	1412(31)		
$\alpha_2(4p_{3/2})$	-109.4(1.1)	-107.9[26]	
$\alpha_2(5p_{3/2})$	-1065(18)		
$\alpha_2(3d_{3/2})$	-482(19)		
$\alpha_2(3d_{5/2})$	-673(23)		

ical value 1. Polarizability in a.u. has the dimension of volume, and its numerical values presented here are expressed in units of  $a_0^3$ , where  $a_0 \approx 0.052918$  nm is the Bohr radius. The atomic units for  $\alpha$  can be converted to SI units via  $\alpha/h$  [Hz/(V/m)<sup>2</sup>]= $2.48832 \times 10^{-8} \alpha$  [a.u.], where the conversion coefficient is  $4\pi\epsilon_0 a_0^3/h$  and the Planck constant  $h$  is factored out.

The frequency-dependent scalar polarizability,  $\alpha(\omega)$ , of an alkali-metal atom in the state  $v$  may be separated into a contribution from the ionic core,  $\alpha_{\text{core}}$ , a core polarizability modification due to the valence electron,  $\alpha_{vc}$ , and a contribution from the valence electron,  $\alpha^v(\omega)$ . The valence contribution to frequency-dependent scalar  $\alpha_0$  and tensor  $\alpha_2$  polarizabilities is evaluated as the sum over intermediate  $k$  states allowed by the electric-dipole transition rules [45]

$$\begin{aligned}
 \alpha_0^v(\omega) &= \frac{2}{3(2j_v+1)} \sum_k \frac{\langle k || d || v \rangle^2 (E_k - E_v)}{(E_k - E_v)^2 - \omega^2}, \\
 \alpha_2^v(\omega) &= -4C \sum_k (-1)^{j_v+j_k+1} \begin{Bmatrix} j_v & 1 & j_k \\ 1 & j_v & 2 \end{Bmatrix} \\
 &\quad \times \frac{\langle k || d || v \rangle^2 (E_k - E_v)}{(E_k - E_v)^2 - \omega^2}, \quad (1)
 \end{aligned}$$

where  $C$  is given by

$$C = \left( \frac{5j_v(2j_v-1)}{6(j_v+1)(2j_v+1)(2j_v+3)} \right)^{1/2}$$

and  $\langle k || d || v \rangle$  are the reduced electric-dipole matrix elements. In these equations,  $\omega$  is assumed to be at least several linewidths off resonance with the corresponding transitions. Linear polarization is assumed in all calculation. The ionic core polarizability and  $\alpha_{vc}$  term depend weakly on  $\omega$  for the frequencies treated here and are approximated by their dc values calculated in the random-

phase approximation (RPA) [45]. We find the contribution from the  $K^+$  ionic core to be  $\alpha_{\text{core}} = 5.457 a_0^3$ . A counter term  $\alpha_{vc}$  compensating for excitation from the core to the valence shell which violates the Pauli principle is very small. For example, it is  $\alpha_{vc} = -0.00015$  a.u. for the  $4p_j$  states of K.

We use the linearized version of the coupled cluster approach (also referred to as the all-order method), which sums infinite sets of many-body perturbation theory terms, for all significant terms in the equations above. The  $4s-np$ ,  $4p-nl$ ,  $5s-nl$ ,  $5p-nl$ , and  $3d-nl$  transitions with  $n \leq 26$  are calculated using this approach [44, 46].

As we noted in the Introduction, the present calculation required evaluation of the electric-dipole matrix elements for highly excited states, since the frequency-dependent polarizabilities for the  $4s-5p$  magic wavelengths of particular experimental interest are dominated by the  $5p-nl$  transitions with  $n = 12-14$ . The difficulty with the applications of the all-order method for these states results from the use a complete set of Dirac-Fock (DF) wave functions on a nonlinear grid generated using B-splines constrained to a spherical cavity. A large cavity with radius of  $R = 220 a_0$  is needed to accommodate all valence orbitals with  $ns = 4s-10s$ ,  $np = 4p-10p$ , and  $nd = 3d-9d$ . A cavity radius of  $400 a_0$  was chosen to accommodate additional valence orbitals with  $ns = 11s-14s$ ,  $np = 11p-13p$ , and  $nd = 10d-12d$ . Our basis set consists of 70 splines of order 11 for each value of the relativistic angular quantum number  $\kappa$  for  $R = 220 a_0$  and 100 splines of order 13 for  $R = 400 a_0$ . We have conducted test comparisons of the basis set energies with the actual DF values to demonstrate the numerical stability of this calculation. We can use available experimental energies for the  $ns = 4s-11s$ ,  $np = 4p-10p$ , and  $nd = 3d-12d$  states from [47] and theoretical all-order energies for other states with  $n \leq 26$ . The remaining small contributions with  $n > 26$  are calculated in the DF approximation. For example, the contributions from states with  $n > 26$  give only 0.075 a.u. to the polarizability of the  $4p_{1/2}$  state. We note that states with  $n > 19$  in our basis have positive energies and provide a discrete representation of the continuum.

The evaluation of the uncertainty of the matrix elements in this approach was described in detail in [32, 44]. Four all-order calculations were carried out, including two *ab initio* all-order calculations with and without the inclusion of the partial triple excitations and two other calculations that incorporated semiempirical estimates of high-order correlation corrections starting from both *ab initio* runs. The spread of these four values for each transition defines the estimated uncertainty in the final results when considered justified based on the dominant correlation contributions to the E1 matrix elements [32, 44]. We note that this procedure does not work in the small number of cases where we can not estimate uncertainty in the dominant contributions using the procedure described above. No uncertainties are listed for such matrix elements, however, their contribu-

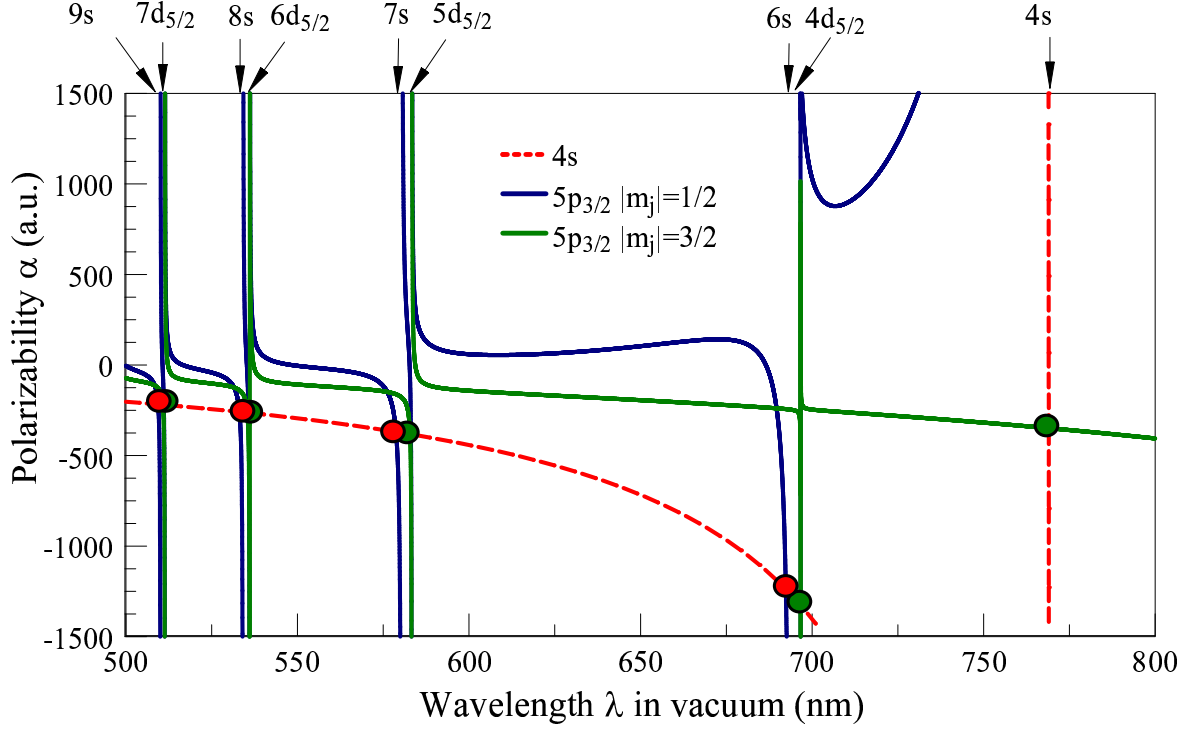


FIG. 1: (Color online) The frequency-dependent polarizabilities of the K  $4s$  and  $4p_{3/2}$  states. The magic wavelengths are marked with circles. The approximate positions of the  $4p_{3/2} - nl$  resonances are indicated by vertical lines with small arrows on top of the graph, together with the corresponding  $nl$ .

tions are small, leading to negligible effects on the final uncertainties of the polarizabilities. The absolute values of the reduced electric-dipole matrix elements used in our subsequent calculations and their uncertainties are listed in a.u. in Table I. We list only the most important subset of the several hundred matrix elements that were calculated in this work.

Our results for scalar and tensor polarizabilities of the  $4p_j$  excited states of potassium are compared with calculations of [48, 49] and with experimental measurements reported by Marrus and Yellin [42] in Table II. The Bates-Damgaard method was used by Schmieder et al. [48] and the time-dependent gauge-invariant variational method was used by Marrus and Yellin [42]. The uncertainty in the experimental measurement [42] of the scalar polarizability is too large to reflect on the accuracy of the present calculations. Extensive comparison of the theoretical and experimental static polarizabilities for the alkali-metal atoms was recently given in the review [45].

#### IV. MAGIC WAVELENGTHS

We define the magic wavelength  $\lambda_{\text{magic}}$  as the wavelength for which the ac polarizabilities of two states involved in the atomic transition are the same, leading to a vanishing ac Stark shift of that transition. For the  $ns - np$  transitions, a magic wavelength is represented by the point at which two curves,  $\alpha_{ns}(\lambda)$  and  $\alpha_{np}(\lambda)$ ,

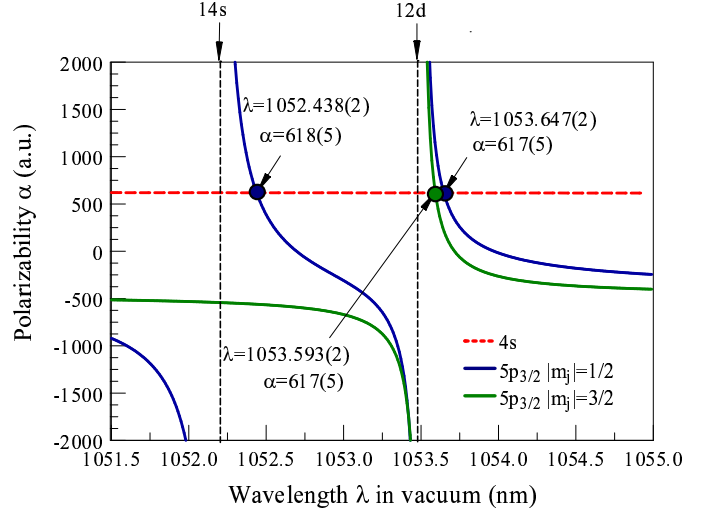


FIG. 2: (Color online) The frequency-dependent polarizabilities of the K  $4s$  and  $5p_{3/2}$  states. The magic wavelengths are marked with circles and arrows. The approximate positions of the  $5p_{3/2} - 14s$  and  $5p_{3/2} - 12d$  resonances are indicated by vertical lines with small arrows on top of the graph.

intersect as a function of the wavelength  $\lambda$ . The total polarizability for the  $np_{3/2}$  states is given by  $\alpha = \alpha_0 - \alpha_2$  for  $m_j = \pm 1/2$  and  $\alpha = \alpha_0 + \alpha_2$  for the  $m_j = \pm 3/2$  case. Therefore, the total polarizability of the  $np_{3/2}$  state depends upon its  $m_j$  quantum number and the magic wavelengths need to be determined separately for the cases

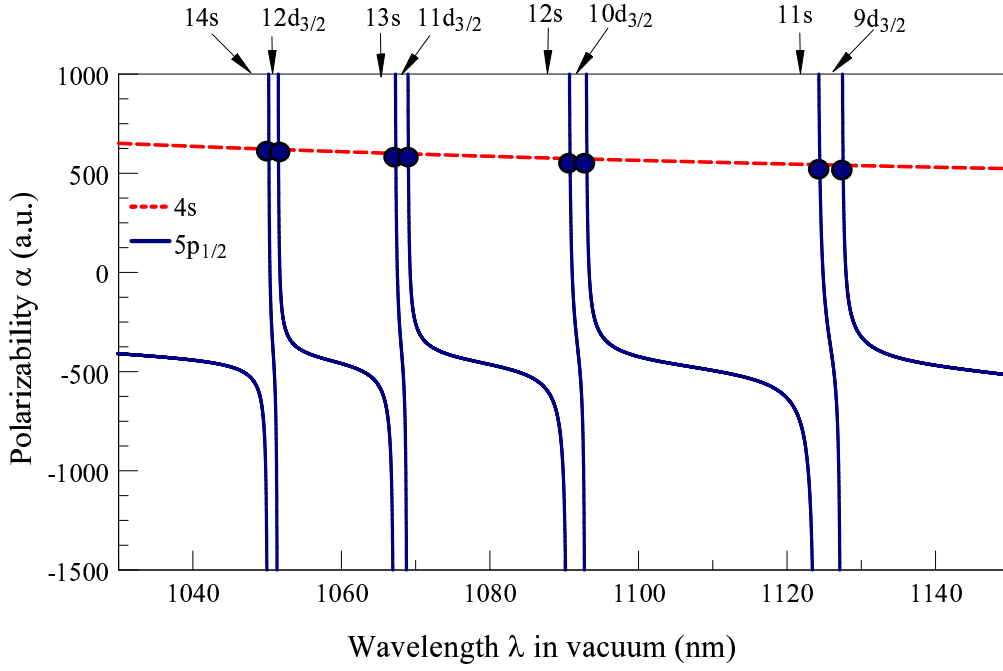


FIG. 3: (Color online) The frequency-dependent polarizabilities of the K  $4s$  and  $5p_{1/2}$  states. The magic wavelengths are marked with circles. The approximate positions of the  $5p_{1/2} - nl$  resonances are indicated by vertical lines with small arrows on top of the graph, together with the corresponding  $nl$ .

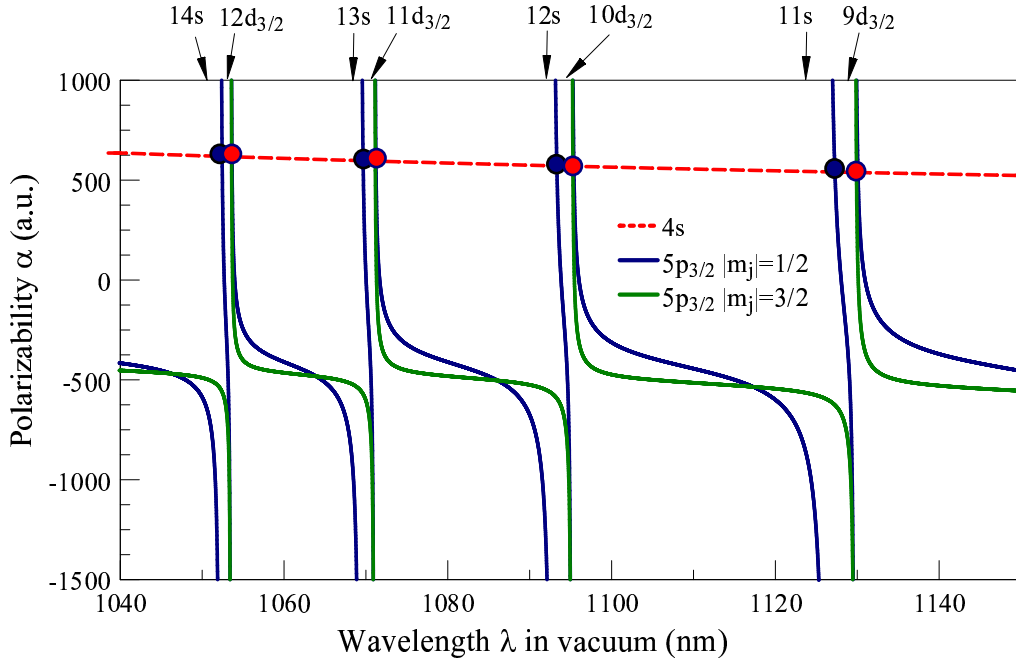


FIG. 4: (Color online) The frequency-dependent polarizabilities of the K  $4s$  and  $5p_{3/2}$  states. The magic wavelengths are marked with circles. The approximate positions of the  $5p_{3/2} - nl$  resonances are indicated by vertical lines with small arrows on top of the graph, together with the corresponding  $nl$ .

TABLE III: Magic wavelengths for the  $4s - np_j$  transitions in K. The 500 – 1227 nm and 1050 – 1130 wavelength ranges were considered for the  $4s - 4p_j$  and  $4s - 5p_j$  transitions, respectively. The corresponding polarizabilities are given in a.u. The resonance near the magic wavelengths are listed in the first column.

Resonance	K $\lambda_{\text{magic}}$	$\alpha$
$4s - 4p_{1/2}$ Transition		
$4p_{1/2} - 9s$	508.12(1)	-215(2)
$4p_{1/2} - 7d_{3/2}$	509.47(1)	-220(3)
$4p_{1/2} - 8s$	531.80(1)	-256(2)
$4p_{1/2} - 6d_{3/2}$	533.99(1)	-260(3)
$4p_{1/2} - 7s$	577.37(1)	-365(3)
$4p_{1/2} - 5d_{3/2}$	581.05(1)	-375(4)
$4p_{1/2} - 6s$	690.17(1)	-1195(10)
$4p_{1/2} - 4s$	768.41(1)	21200(400)
$4p_{1/2} - 5s, 3d_{3/2}$	1227.63(2)	475(40)
$4s - 4p_{3/2},  m_j  = 1/2$ Transition		
$4p_{3/2} - 9s$	509.38(1)	-217(2)
$4p_{3/2} - 7d_{5/2}$	511.04(1)	-220(2)
$4p_{3/2} - 8s$	533.07(1)	-259(2)
$4p_{3/2} - 6d_{5/2}$	535.72(1)	-264(2)
$4p_{3/2} - 7s$	578.71(1)	-369(3)
$4p_{3/2} - 5d_{5/2}$	583.07(1)	-383(3)
$4p_{3/2} - 6s$	692.35(1)	-1237(12)
$4p_{3/2} - 4s$	769.43(1)	-27400(200)
$4p_{3/2} - 5s, 3d_j$	1227.61(1)	475(45)
$4s - 4p_{3/2},  m_j  = 3/2$ Transition		
$4p_{3/2} - 7d_{5/2}$	510.75(1)	-319(2)
$4p_{3/2} - 6d_{5/2}$	535.38(1)	-263(3)
$4p_{3/2} - 5d_{5/2}$	582.80(1)	-383(3)
$4s - 4p_j$	768.98(2)	-367
$4s - 5p_{1/2}$ Transition		
$5p_{1/2} - 14s$	1050.238(2)	620(5)
$5p_{1/2} - 12d_{3/2}$	1051.528(2)	620(5)
$5p_{1/2} - 13s$	1067.326(2)	600(5)
$5p_{1/2} - 11d_{3/2}$	1069.017(2)	598(5)
$5p_{1/2} - 12s$	1090.784(4)	574(5)
$5p_{1/2} - 10d_{3/2}$	1093.057(3)	572(5)
$5p_{1/2} - 11s$	1124.419(6)	543(5)
$5p_{1/2} - 9d_{3/2}$	1127.560(6)	540(5)
$4s - 5p_{3/2},  m_j  = 1/2$ Transition		
$5p_{3/2} - 14s$	1052.438(2)	618(5)
$5p_{3/2} - 12d_{3/2}$	1053.647(2)	617(5)
$5p_{3/2} - 13s$	1069.656(3)	597(5)
$5p_{3/2} - 11d_{3/2}$	1071.224(3)	595(5)
$5p_{3/2} - 12s$	1093.312(4)	571(5)
$5p_{3/2} - 10d_{3/2}$	1095.393(4)	569(5)
$5p_{3/2} - 11s$	1127.275(8)	540(5)
$5p_{3/2} - 9d_{3/2}$	1130.092(8)	538(5)
$4s - 5p_{3/2},  m_j  = 3/2$ Transition		
$5p_{3/2} - 12d_{3/2}$	1053.593(2)	617(5)
$5p_{3/2} - 11d_{3/2}$	1071.144(2)	595(5)
$5p_{3/2} - 10d_{3/2}$	1095.274(3)	569(5)
$5p_{3/2} - 9d_{3/2}$	1129.908(4)	538(5)

with  $m_j = \pm 1/2$  and  $m_j = \pm 3/2$  for the  $ns - np_{3/2}$  transitions, owing to the presence of the tensor contribution to the total polarizability of the  $np_{3/2}$  state. The uncertainties in the values of magic wavelengths are found as the maximum differences between the central value and the crossings of the  $\alpha_{ns} \pm \delta\alpha_{ns}$  and  $\alpha_{np} \pm \delta\alpha_{np}$  curves, where the  $\delta\alpha$  are the uncertainties in the corresponding  $ns$  and  $np$  polarizability values. All calculations are carried out for linear polarization. Several magic wavelengths were calculated for the  $4s - 4p_{1/2}$  and  $4s - 4p_{3/2}$  transitions in K in Ref. [14] using the all-order approach. Only the magic wavelengths with  $\lambda > 600$  nm were listed. In this work, we present several other magic wavelengths for these  $D_1, D_2$  transitions above 500 nm.

The frequency-dependent polarizabilities of the  $4s$  and  $4p_{3/2}$  states for  $\lambda = 500 - 800$  nm are plotted in Fig. 1. The magic wavelengths are marked with circles. The approximate positions of the  $4p_{3/2} - nl$  resonances are indicated by vertical lines with small arrows on top of the graph, together with the corresponding  $nl$ . For example, the arrow labelled  $7s$  indicates the position of the  $4p_{3/2} - 7s$  resonance. The corresponding magic wavelengths are listed in Table III. We note that the  $4p_{3/2} - 5s$  resonance wavelength is outside of the plot region at  $\lambda = 1253$  nm). While there are 8 magic wavelengths for the  $4s - 4p_{3/2} |m_j| = 1/2$  transition in the wavelength region shown on the plot, there are only 4 magic wavelengths for the  $4s - 4p_{3/2} |m_j| = 3/2$  transition since there are no corresponding crossings near the  $4p_{3/2} - ns$  resonances as in the case of  $|m_j| = 1/2$ . The 769 nm magic wavelength for the  $|m_j| = 1/2$  is not shown on the plot since the corresponding polarizability (-27400 a.u.) is outside of the plot y-axis range. There is only one magic wavelength above 800 nm for the  $4s - 4p_{3/2} |m_j| = 1/2$  transition due to  $4p_{3/2} - 5s$  resonance and none for the  $|m_j| = 3/2$  case. The magic wavelengths for the  $4s - 4p_{1/2}$  transition are very close to those for  $4s - 4p_{3/2} |m_j| = 1/2$ . They are also given in Table III.

The magic wavelengths for the UV  $4s - 5p_j$  transitions are completely different than those for the  $D_1, D_2$  lines owing to completely different set of resonances. The K case is also significantly different from that of Li [32] due to differences in the resonant transition wavelengths. We list the magic wavelengths for the  $4s - 5p_{1/2}$  and  $4s - 5p_{3/2}$  transitions in the range of 1050-1130 nm, which is of particular experimental interest in Table III. We find 20 magic wavelengths in the technically interest region of 1050 – 1130 nm accessible by a number of widely used lasers. The magic wavelengths for the  $4s - 5p_{3/2}$  transition near 1053 nm wavelength are illustrated in Fig. 2. As in the case of the  $4s - 4p_{3/2}$  transition, there is no magic wavelength for the  $|m_j| = 1/2$  case near the  $ns$  resonance. All magic wavelengths for the  $4s - 5p_{1/2}$  and  $4s - 5p_{3/2}$  transitions in the range of 1050-1140 nm are illustrated in Figs. 3 and Figs. 4. The same designations are used as in the previous graphs. Comparing these figures with the similar plots for Li (see Figs. 3 and 4 of Ref. [32]) shows

that K magic wavelengths near 1050-1130 nm originate from crossings near much higher resonances ( $n = 9 - 14$  vs.  $n = 6 - 7$  for Li) making the calculation for K more complicated due to the very large cavity size required to accommodate such highly excited orbitals.

## V. CONCLUSION

We have calculated the ground  $4s$ ,  $4p$ , and  $5p$  state ac polarizabilities in K using the relativistic linearized coupled-cluster method and evaluated the uncertainties of these values. We have used our calculations to iden-

tify the magic wavelengths for the  $4s - 4p$  and  $4s - 5p$  transitions. The magic wavelengths for the ultraviolet resonance lines is of particular interest for laser cooling of ultracold gases with high phase-space densities.

## Acknowledgement

This research was performed under the sponsorship of the US Department of Commerce, National Institute of Standards and Technology, and was supported by the National Science Foundation under Physics Frontiers Center Grant PHY-0822671.

- 
- [1] L. Yi, S. Mejri, J. McFerran, Y. Le Coq, and S. Bize, *Phys. Rev. Lett.* **106**, 073005 (2011).
  - [2] D. C. McKay, D. Jervis, D. J. Fine, J. W. Simpson-Porco, G. J. A. Edge, and J. H. Thywissen, *Phys. Rev. A* **84**, 063420 (2011).
  - [3] N. Lundblad, M. Schlosser, and J. Porto, *Phys. Rev. A* **81**, 031611 (2010).
  - [4] J. McFerran, S. Mejri, L. Yi, and S. Bize, 2010 Conference on Precision Electromagnetic Measurements (CPEM 2010) pp. 85 – 6 (2010).
  - [5] A. Derevianko, *Phys. Rev. Lett.* **105**, 033002 (2010).
  - [6] H. Katori, K. Hashiguchi, E. Il'inova, and V. Ovsiannikov, *Phys. Rev. Lett.* **103**, 153004 (2009).
  - [7] V. Dzuba, V. Flambaum, and B. Lev, *Phys. Rev. A* **83**, 032502 (2011).
  - [8] S. Zhang, F. Robicheaux, and M. Saffman, *Phys. Rev. A* **84**, 043408 (2011).
  - [9] U. Dammalapati, B. Santra, and L. Willmann, *J. Phys. B* **45**, 025001 (2012).
  - [10] Y. Geng-Hua, Z. Jia-Qi, L. Run-Bing, W. Jin, and Z. Ming-Sheng, *Chin. Phys. Lett.* **28**, 073201 (2011).
  - [11] M. Safronova, D. Jiang, M. Kozlov, and U. Safronova, 2010 IEEE International Frequency Control Symposium (FCS) p. 59 (2010).
  - [12] A. Ye and G. Wang, *Phys. Rev. A* **78**, 014502 (2008).
  - [13] K. Guo, G. Wang, and A. Ye, *J. Phys. B* **43**, 135004 (2010).
  - [14] B. Arora, M. Safronova, and C. W. Clark, *Phys. Rev. A* **76**, 052509 (2007).
  - [15] Z. Yu-Nan, Z. Xiao-Ji, C. Jing-Biao, and C. Xu-Zong, *Chin. Phys. Lett.* **23**, 1687 (2006).
  - [16] H. Katori, T. Ido, and M. Kuwata-Gonokami, *J. Phys. Soc. Jpn.* **66**, 2479 (1999).
  - [17] J. Ye, D. W. Vernooy, and H. J. Kimble, *Phys. Rev. Lett.* **83**, 4987 (1999).
  - [18] P. M. Duarte, R. A. Hart, J. M. Hitchcock, T. A. Corcovilos, T.-L. Yang, A. Reed, and R. G. Hulet, *Phys. Rev. A* **84**, 061406(R) (2011).
  - [19] J. McKeever, J. R. Buck, A. D. Boozer, A. Kuzmich, H.-C. Nägerl, D. M. Stamper-Kurn, and H. J. Kimble, *Phys. Rev. Lett.* **90**, 133602 (2003).
  - [20] M. S. Safronova, C. J. Williams, and C. W. Clark, *Phys. Rev. A* **67**, 040303 (2003).
  - [21] M. Saffman and T. G. Walker, *Phys. Rev. A* **72**, 022347 (2005).
  - [22] B. Arora, M. S. Safronova, and C. W. Clark, *Phys. Rev. A* **82**, 022509 (2010).
  - [23] L. J. Leblanc and J. H. Thywissen, *Phys. Rev. A* **75**, 053612 (2007).
  - [24] B. Arora, M. S. Safronova, and C. W. Clark, *Phys. Rev. A* **84**, 043401 (2011).
  - [25] W. F. Holmgren, M. C. Revelle, V. P. A. Lonij, and A. D. Cronin, *Phys. Rev. A* **81**, 053607 (2010).
  - [26] U. I. Safronova and M. S. Safronova, *Phys. Rev. A* **78**, 052504 (2008).
  - [27] G. K. Brennen, I. H. Deutsch, and P. S. Jessen, *Phys. Rev. A* **61**, 062309 (2000).
  - [28] M. Saffman, T. G. Walker, and K. Mølmer, *Rev. Mod. Phys.* **82**, 2313 (2010).
  - [29] S. Falke, I. Sherstov, E. Tiemann, and C. Lisdat, *J. Chem. Phys.* **125**, 224303 (2006).
  - [30] B. Arora and B. K. Sahoo, *Phys. Rev. A* **86**, 033416 (2012).
  - [31] B. K. Sahoo and Bindiya Arora, arXiv:1212.1814 [physics.atom-ph].
  - [32] M. S. Safronova, U. I. Safronova, and C. W. Clark, *Phys. Rev. A* **86**, 042505 (2012).
  - [33] A. D. Ludlow, T. Zelevinsky, G. K. Campbell, S. Blatt, M. M. Boyd, M. H. G. de Miranda, M. J. Martin, J. W. Thomsen, S. M. Foreman, J. Ye, et al., *Science* **319**, 1805 (2008).
  - [34] T. Ido and H. Katori, *Phys. Rev. Lett.* **91**, 053001 (2003).
  - [35] S. G. Porsev, A. Derevianko, and E. N. Fortson, *Phys. Rev. A* **69**, 021403 (2004).
  - [36] Z. W. Barber, J. E. Stalnaker, N. D. Lemke, N. Poli, C. W. Oates, T. M. Fortier, S. A. Diddams, L. Hollberg, C. W. Hoyt, A. V. Taichenachev, et al., *Phys. Rev. Lett.* **100**, 103002 (2008).
  - [37] H. Hachisu, K. Miyagishi, S. G. Porsev, A. Derevianko, V. D. Ovsiannikov, V. G. Pal'Chikov, M. Takamoto, and H. Katori, *Phys. Rev. Lett.* **100**, 053001 (2008).
  - [38] A. Derevianko, B. Obreshkov, and V. A. Dzuba, *Phys. Rev. Lett.* **103**, 133201 (2009).
  - [39] M. S. Safronova, S. G. Porsev, and C. W. Clark, *Phys. Rev. Lett.* **109**, 230802 (2012).
  - [40] M. S. Safronova, S. G. Porsev, U. I. Safronova, M. G. Kozlov, and Charles W. Clark, arXiv:1210.7272, submitted to *Phys. Rev. A* (2012).
  - [41] A. Derevianko, W. R. Johnson, M. S. Safronova, and J. F. Babb, *Phys. Rev. Lett.* **82**, 3589 (1999).



- [42] R. Marrus and J. Yellin, Phys. Rev. **177**, 127 (1969).
- [43] W. R. Johnson, U. I. Safronova, A. Derevianko, and M. S. Safronova, Phys. Rev. A **77**, 022510 (2008).
- [44] M. S. Safronova and U. I. Safronova, Phys. Rev. A **83**, 052508 (2011).
- [45] J. Mitroy, M. S. Safronova, and C. W. Clark, J. Phys. B **43**, 202001 (2010).
- [46] M. S. Safronova and W. R. Johnson, Adv. At. Mol. Opt. Phys. **55**, 191 (2008).
- [47] Yu. Ralchenko, A. Kramida, J. Reader, and NIST ASD Team (2011). NIST Atomic Spectra Database (version 4.1), [Online]. Available: <http://physics.nist.gov/asd>. National Institute of Standards and Technology, Gaithersburg, MD.
- [48] R. Schmieder, A. Lurio, and W. Happer, Phys. Rev. A **3**, 1209 (1971).
- [49] M. Méréwa and D. Bégué, J. Chem. Phys. **108**, 5289 (1998).